SEE COMMENTARY

Differential fates of biomolecules delivered to target cells via extracellular vesicles

Masamitsu Kanada[a], Michael H. Bachmann[a], Jonathan W. Hardy[a], Daniel Omar Frimannson[b], Laura Bronsart[a], Andrew Wang[a], Matthew D. Sylvester[b], Tobi L. Schmidt[a], Roger L. Kaspar[c], Manish J. Butte[a], A. C. Matin[b], and Christopher H. Contag[a,b,d,1]

Departments of [a]Pediatrics, [b]Microbiology and Immunology, and [d]Radiology, Stanford University School of Medicine, Stanford, CA 94305; and [c]TransDerm Inc., Santa Cruz, CA 95060

Edited by Gregg L. Semenza, The Johns Hopkins University School of Medicine, Baltimore, MD, and approved January 20, 2015 (received for review September 25, 2014)

Extracellular vesicles (EVs), specifically exosomes and microvesicles (MVs), are presumed to play key roles in cell–cell communication via transfer of biomolecules between cells. The biogenesis of these two types of EVs differs as they originate from either the endosomal (exosomes) or plasma (MVs) membranes. To elucidate the primary means through which EVs mediate intercellular communication, we characterized their ability to encapsulate and deliver different types of macromolecules from transiently transfected cells. Both EV types encapsulated reporter proteins and mRNA but only MVs transferred the reporter function to recipient cells. De novo reporter protein expression in recipient cells resulted only from plasmid DNA (pDNA) after delivery via MVs. Reporter mRNA was delivered to recipient cells by both EV types, but was rapidly degraded without being translated. MVs also mediated delivery of functional pDNA encoding Cre recombinase in vivo to tissues in transgenic Cre-lox reporter mice. Within the parameters of this study, MVs delivered functional pDNA, but not RNA, whereas exosomes from the same source did not deliver functional nucleic acids. These results have significant implications for understanding the role of EVs in cellular communication and for development of EVs as delivery tools. Moreover, studies using EVs from transiently transfected cells may be confounded by a predominance of pDNA transfer.

cell communication | extracellular vesicle | exosome | microvesicle | apoptotic body

Extracellular vesicles (EVs) are naturally secreted by most cells into the extracellular environment, and although their designations remain controversial, EVs have been classified as either exosomes or microvesicles (MVs), based on their size, composition, and biogenesis (1–3). EVs have been implicated in important biological processes such as surface-membrane trafficking and horizontal transfer of proteins and RNAs among neighboring cells, and even to cells at distant tissue sites (4–11). Exosomes are generally thought to be 40–120 nm in diameter and secreted from endosomal compartments called multivesicular bodies (MVBs). MVs are, by and large, considered to be 50–1,000 nm in diameter and created through direct budding from the cellular plasma membrane. Although these characteristics can be variable when comparing EVs from divergent sources, there is some consistency of distinct identification when deriving them from a single cell type under controlled conditions. Recently, some of the molecular mechanisms involved in EV biogenesis and secretion have been reported, including plasma membrane budding of MVs (12), microRNA (miRNA) sorting (13), intraluminal budding (14), and MVB docking to the plasma membrane (15). However, after they are generated and in the extracellular space, little is known about the fate of EVs, the molecular mechanisms mediating EV uptake in near and distant recipient cells, or the fates of molecular cargo that is carried into cells. Understanding the fate of EVs and their cargo are crucial to revealing EV function and for the development of EV-mediated therapies.

Toward these ends, we report here differential loading of nucleic acids including plasmid DNA (pDNA), mRNA, and siRNA into exosomes and MVs. We further demonstrate that, under the constraints of our experimental approach, MVs but not exosomes derived from cells transiently transfected with pDNA, induced the subsequent expression of encoded reporter proteins in recipient cells. We also observed that loading of mRNA and siRNA into MVs was more efficient than into exosomes, and that even though mRNA was delivered by MVs into recipient cells, it was rapidly degraded without being translated into protein. Likewise, siRNAs delivered to recipient cells did not reduce expression of target molecules significantly. Finally, we demonstrate, in vivo, the transfer of functional biomolecules via tumor cell-derived MVs, using pDNA encoding Cre recombinase to convert cells in transgenic Cre-lox Luc reporter mice. These data indicated that MVs from transiently transfected cells contained pDNA, mRNA, and protein, but of these, only pDNA was functional following transfer to recipient cells. In contrast to MVs, exosomes could not deliver functional nucleic acids of any kind. Our observations suggest that the pathways through which EVs enter cells dramatically impact EV-mediated biomolecule delivery. These results explain some of the observations reported in the field, influence our understanding of the role EVs play in biology, and affect the way we think of using EVs in diagnostics and therapy.

Significance

Extracellular vesicle (EV)-mediated transfer of macromolecules may play a key role in cellular communication and may have utility in directed molecular therapies. In addition, the EV packaged biomolecules in serum may have potential for diagnosing cancer and determining its likelihood of metastasis. EVs are heterogeneous and there are many outstanding questions associated with biogenesis, uptake, and the fate of transferred molecules in recipient cells. In fact, the function, characterization, and even the nomenclature of EVs are being refined. Here we aimed to improve the functional characterization of EVs, and observed that only microvesicles (MVs), but not exosomes, can functionally transfer loaded reporter molecules to recipient cells, largely by delivering plasmid DNA. Our data show that exosomes and MVs are structurally and functionally distinct.

Author contributions: M.K., M.H.B., J.W.H., D.O.F., A.W., R.L.K., M.J.B., A.C.M., and C.H.C. designed research; M.K., J.W.H., D.O.F., L.B., A.W., M.D.S., and T.L.S. performed research; M.K., M.H.B., J.W.H., D.O.F., A.W., and C.H.C. analyzed data; and M.K., M.H.B., J.W.H., D.O.F., A.W., R.L.K., M.J.B., A.C.M., and C.H.C. wrote the paper.

The authors declare no conflict of interest.

This article is a PNAS Direct Submission.

See Commentary on page 3589.

[1]To whom correspondence should be addressed. Email: ccontag@stanford.edu.

This article contains supporting information online at www.pnas.org/lookup/suppl/doi:10.1073/pnas.1418401112/-/DCSupplemental.

CELL BIOLOGY

Results

Isolation and Characterization of Exosomes and MVs. We isolated EVs from conditioned medium of HEK293FT cells by differential ultracentrifugation (Fig. 1*A*), as previously described and well studied (16). The proteins from isolated EVs were initially characterized on Western blots to assess expression of the marker protein, CD63. Unexpectedly, the amount of glyceraldehyde 3-phosphate dehydrogenase (GAPDH), which is typically used as an internal control for cellular proteins, was consistently lower in the MV fraction than the exosome fraction, despite loading equal amounts of protein; this result likely reflects differences in biogenesis. In fact, we could not find a protein that is equally loaded into both EV fractions to normalize the analyses in this study, and thus we relied on protein content and particle counting for uniformity. The exosomes from the HEK293FT cells showed significant CD63 expression, whereas this marker was not detected in the MV fraction (Fig. 1*B*); this finding is consistent with previous reports (17). This observation also indicated that the exosome and MV fractions isolated with this protocol were molecularly distinct. EVs in these fractions were further analyzed by size using dynamic light scattering (DLS). Both the exsome and MV preparations showed single bell-shaped size distributions (Fig. 1 *C* and *D*), with peaks of 165 nm (exosomes) and 232 nm (MVs). Herein, we refer to the smaller EVs from HEK293FT prepared in this manner as exosomes, and the larger EVs as MVs. Unexpectedly, however, the sizes of exosomes and MVs determined by DLS were very similar, and the peak size of exosomes was 37.5% larger than the upper limit of its typically reported size range, 40–120 nm. Hence, these fractions were also analyzed by nanoparticle tracking analysis (NTA). NTA showed peak sizes that were more similar in size than those measured by DLS, with peaks of 151 nm (exosomes) and 156 nm (MVs). In addition, a smaller peak at 43 nm was also observed in the exosome fraction (*SI Appendix*, Fig. S1). The concentration of particles was 50×10^8 particles/mL (exosomes) and 52×10^8 particles/mL (MVs) in this analysis. The quantification and sizing revealed that many exosomes and MVs have similar sizes, but that the density of the MV fraction is greater than that of the exosome fraction because these fractions had been separated by differential ultracentrifugation. These data further suggest that size alone cannot always distinguish exosomes from MVs, and molecular markers should be used.

To further characterize the size, nanostructure, and physical properties of individual EVs, we imaged isolated exosomes and MVs immobilized on mica surfaces by atomic force microscopy (AFM). Without $MgCl_2$, only MVs, but not exosomes, could be immobilized on the negatively charged mica surface at 30 min, also evidence of distinct molecular composition. Most immobilized MVs remained intact but showed a flattened appearance; however, there was also evidence of collapsed MVs (Fig. 1 *F* and *H*). Because the electrostatic interaction between phospholipids and mica surfaces is altered in the presence of cations (18), we evaluated the effects of Mg^{2+} on EV immobilization on the mica surface. Addition of 10 mM $MgCl_2$ facilitated absorption for both exosomes and MVs. In 30 min, most of the MVs that had absorbed onto the surface collapsed into flat lipid-bilayer patches (*SI Appendix*, Fig. S2). Exosomes, on the other hand, remained intact for the most part, but showed a flattened appearance, as did MVs without Mg^{2+} (Fig. 1 *E* and *G*). From the topographic image, the volumes (V) of individual exosomes and MVs were calculated and their intact diameter (d) was obtained from the equation $V = \pi d^3/6$, assuming a spherical morphology. The diameters of three individual exosomes in Fig. 1*E* were determined to be 84, 53, and 77 nm, whereas three individual MVs (Fig. 1*F*) measured 130, 123, and 99 nm in diameter, respectively. This size range falls within that observed by both DLS and NTA, albeit more consistent with the NTA data, which revealed a smaller population of EV in the exosome fraction. Our AFM results suggest that exosomes and MVs isolated from HEK293FT cells by differential ultracentrifugation differ in volume and surface charge properties, in addition to their distinct molecular composition. As noted above, the size distribution of exosomes and MVs is complex, and different methods measuring this distribution in the same sample can yield slightly different results.

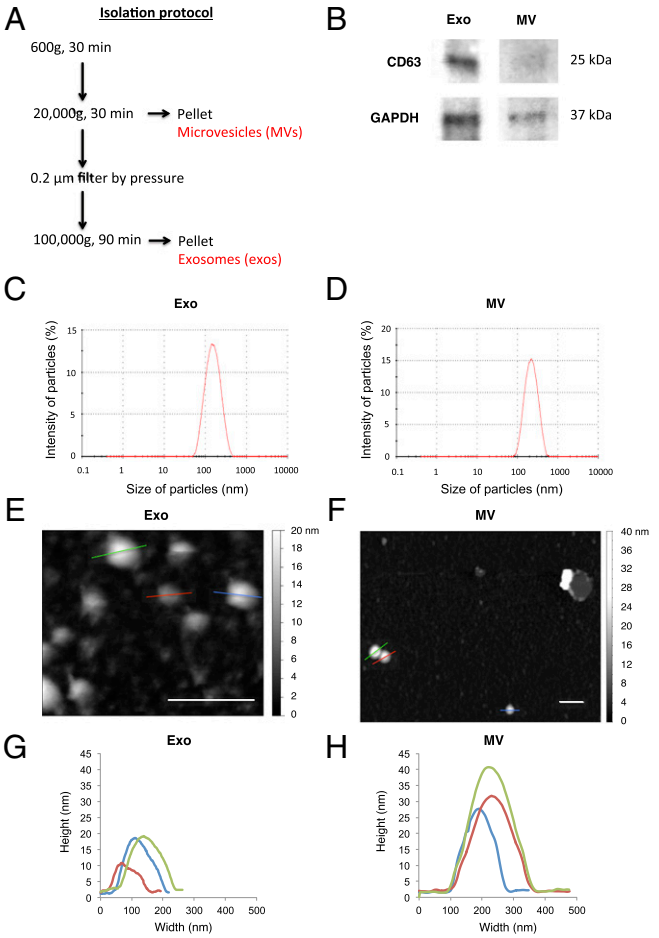

Fig. 1. Size, surface markers, and physical characteristics of EVs. (*A*) Schematic depiction of the isolation protocol for exosomes and MVs. (*B*) Western blot analysis of the exosome marker protein, CD63. Detection of GAPDH was used as a loading control. (*C* and *D*) Size distribution of exosomes and MVs measured by DLS. (*E* and *F*) Topographic AFM images of exosomes and MVs adsorbed to the mica surface. Arrow indicates collapsed MV and lipid-bilayer spreading on the mica surface. (Scale bars, 400 nm.) (*G* and *H*) Size distribution of three randomly chosen exosomes and MVs imaged by AFM.

Encapsulation of Reporter Proteins by Exosomes and MVs, and Uptake by Recipient Cells. To evaluate differential reporter protein loading of exosomes and MVs, these vesicles must be distinguished on a molecular level. EVs were prepared from conditioned medium of HEK293FT cells transiently expressing a fusion protein composed of a firefly luciferase (Luc), and the red fluorescent protein (RFP), tandem Tomato (tdTomato) (19). Both types of EVs prepared from these cells showed red fluorescence, indicating that the fusion protein was loaded into both EVs during vesicle biogenesis (*SI Appendix*, Fig. S3*A*). Loading efficiencies of the fusion protein were measured with a luciferase assay, showing that MVs contained 2.6 times more Luc protein per milligram of total protein than exosomes (*SI Appendix*, Fig. S3*B*). The fraction of exosomes that contained the RFP was confirmed using flow cytometry and costaining for the CD63 surface protein. The

analyses showed that 57.1 ± 8.5% (average ± SD) of the CD63 antibody-coated beads captured the RFP-containing exosomes, whereas 3.3 ± 0.4% captured the RFP-containing MVs (*SI Appendix*, Fig. S3*C*).

To further distinguish the exosome and MV populations on a molecular level, annexin staining was used. Phosphatidylserine (PS) externalization accompanies the shedding of plasma membrane-derived MVs (12), and therefore the outer membrane leaflets of MVs can be stained with FITC-conjugated annexin V, a high-affinity PS-binding protein (5, 17). After staining EVs with annexin V, we observed that 89.5 ± 0.7% (average ± SD) of exosomes showed RFP fluorescence only (Fig. 2 *A* and *C*), whereas 78.7 ± 7.5% of MVs displayed both RFP and FITC fluorescence (Fig. 2 *B* and *D*). To rule out the possibility that FITC nonspecifically binds to MVs, we used FITC-dextran as a control and demonstrated that it does not stain MVs (*SI Appendix*, Fig. S4). These data indicated that the membranes of the vesicles in the MV fraction have exposed PS, but this was not observed for vesicles in the exosome fraction.

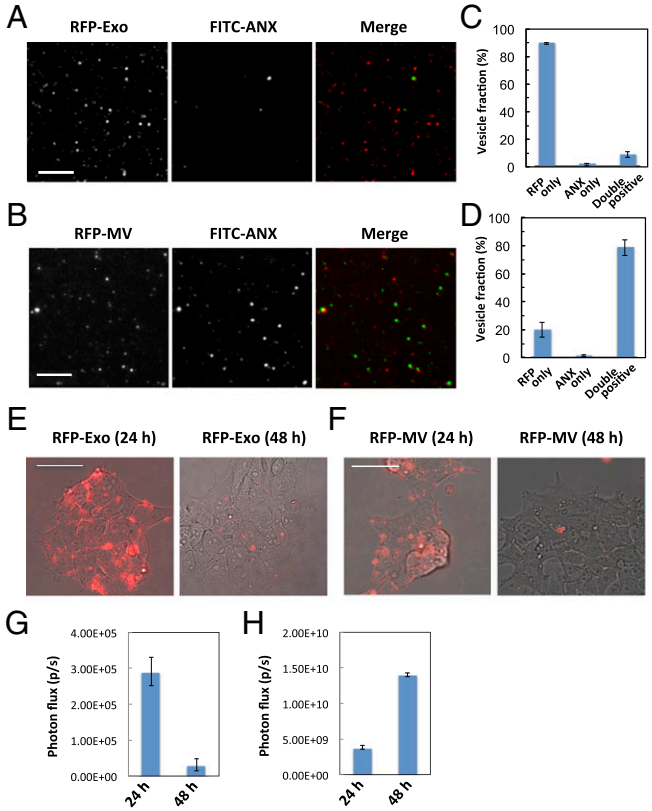

Fig. 2. Membrane lipid composition of EVs and uptake by recipient cells. (*A* and *B*) Detection of fluorescent protein and phosphatidylserine (PS) in EVs. Loaded RFP was visualized by fluorescence (*Left*) and pseudocolor rendered red in the merged images (*Right*). PS in the outer membranes of EVs derived from HEK293FT cells was stained with FITC-annexin V (*Middle*, green in the merged images). (Scale bars, 10 μm.) (*C* and *D*) Fraction of the EVs that contain RFP only, stain with annexin V (ANX) only, or exhibiting both signals. Two hundred vesicles were counted. Error bars represent SD (n = 3). (*E* and *F*) Merged images of fluorescence of RFP-containing EVs and phase contrast images of the recipient HEK293FT cells. The EVs were cultured with the recipient cells for 24 h (labeled as 24 h). The recipient cells were cultured for another 24 h after removing the nonadherent EVs (labeled as 48 h). (Scale bars, 50 μm.) (*G* and *H*) Evaluation of delivered Luc protein in the recipient cells. A total of 0.5 μg of the Luc–RFP-containing EVs were cultured with the cells as described in *E* and *F*. The recipient cells were lysed at 24 or 48 h, respectively, and Luc activity was measured. Error bars represent SD (n = 3).

To assess protein delivery via MVs, RFP-containing exosomes and MVs were added to recipient cells. Despite different characteristics of EVs, both labeled exosomes and MVs were taken up by recipient HEK293FT cells without any significant difference in levels of RFP fluorescence noted at 24 h (Fig. 2 *E* and *F*). The RFP signal in recipient cells for each EV type exhibited a punctate pattern, suggesting uptake of intact EVs rather than fusion with the plasma membrane and immediate release of the contents. Floating, nonadherent EVs were removed from cultures of recipient cells and the cells were incubated for another 24 h. Unexpectedly, fluorescence from RFP delivered by EVs was nearly undetectable at this time point (Fig. 2 *E* and *F*). The amount of delivered reporter Luc–RFP fusion protein was then quantified using a luciferase assay. Significant bioluminescence signals were only detected after lysing the recipient cells treated with reporter protein-containing exosomes. This result suggests that at 24 h, exosomes were intact and fluorescent in the cells; however, access to ATP, needed for firefly luciferase activity, was limiting because no bioluminescence was observed until the cells were lysed and ATP was provided. The Luc–RFP protein in the recipient cells treated with reporter-containing exosomes decreased to 10.7% at 48 h (Fig. 2*G*) as observed by fluorescence microscopy (as in Fig. 2*E*), whereas the cells treated with Luc-containing MVs increased by 365.8% over this time frame (Fig. 2*H*).

It has been noted that exosomes can be stained with lipophilic dyes, leading to perinuclear staining patterns (20). However, cell membrane components that bind the dyes may be recycled after EV degradation, resulting in staining of other intracellular compartments over time. To evaluate this process, we stained EVs with the lipophilic, red fluorescent dye, PKH26 (21), and incubated the stained EVs with recipient HEK293FT cells. Nonadherent EVs were removed and cells were cultured for 24 h. After 24 h, PKH26 fluorescence was observed in subcellular compartments of the recipient cells, in contrast to no fluorescence being detected in cells treated with RFP-containing EVs without PKH26 (*SI Appendix*, Fig. S5). These results suggested that both exosomes and MVs are taken up by recipient cells and then fuse with intercellular compartments.

MV-Mediated Delivery of Nucleic Acids for de Novo Expression of Reporter Protein in Recipient Cells. To investigate the capacity of EVs to deliver functional nucleic acids, recipient HEK293FT cells were cultured with exosomes or MVs derived from transfected donor cells transiently expressing the fusion protein Luc–RFP. Delivery of reporter molecules was evaluated by bioluminescence imaging (BLI) of live cells and fluorescence. Surprisingly, only the MVs led to Luc–RFP expression in the recipient HEK293FT cells as detected by live-cell BLI, even though both types of EVs encapsulated the reporter proteins (Fig. 3*A*). After the MV-mediated transfer, the bioluminescence signal increased over 3 d (Fig. 3*B*), suggesting that nucleic acids were delivered, leading to de novo expression of reporter proteins in recipient cells and increased signal. HEK293FT cells transfected by lipofection (Lipofectamine 2000) with Luc-encoding pDNA showed a different time course of Luc expression than cells labeled by MV-mediated delivery (*SI Appendix*, Fig. S6). This observation suggested that the mechanism of MV-mediated delivery of nucleic acids and protein expression may be different from that of cationic lipid-based delivery of pDNA, which is typically used for transfection (22). To analyze the molecular transfer at the level of individual cells, the recipient cells were also observed by bioluminescence microscopy on day 3. The cells treated with Luc–RFP-containing exosomes showed no detectable bioluminescence, whereas Luc–RFP-containing MVs led to bioluminescence in the recipient cells (Fig. 3*C*). The number of cells expressing the RFP on day 3 was also determined by flow cytometry, showing that 5.5 ± 3.1% (average ± SD) of the recipient cells treated with Luc–RFP-containing MVs showed RFP expression.

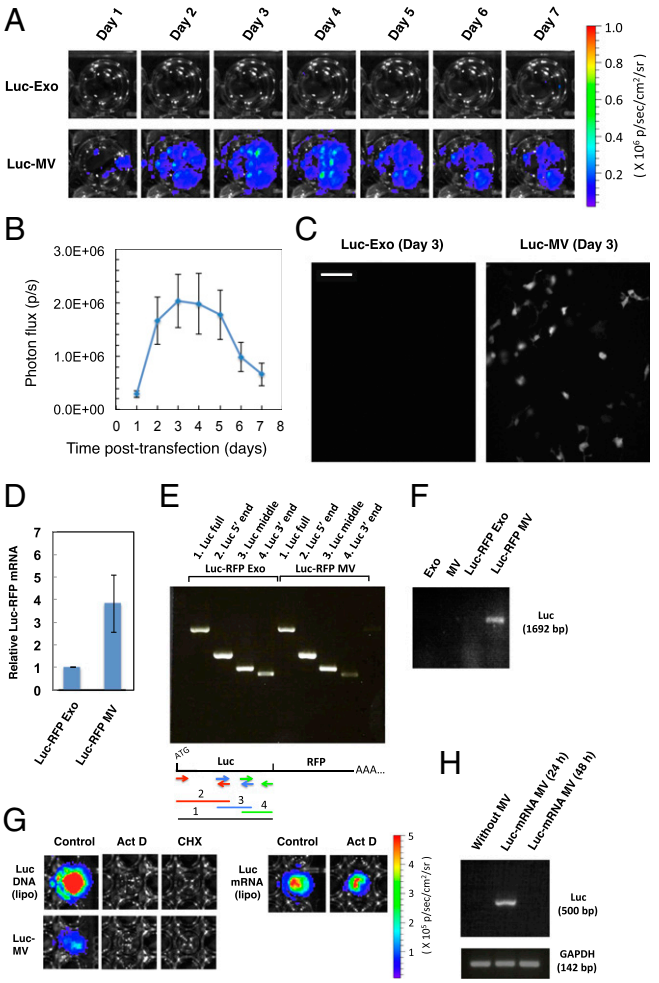

Fig. 3. MV-mediated delivery of pDNA. (*A*) Bioluminescence in EV-treated HEK293FT cells. (*Upper*) HEK293FT cells were treated with 0.4 μg exosomes derived from HEK293FT cells transiently transfected with Luc–RFP expression vector. (*Lower*) Recipient cells were treated with 0.4 μg MVs from the same donor cells. The color scale indicates radiance (x10^6 photons/cm^2/s/sr). (*B*) Time course of bioluminescence in the recipient cells that took up Luc–RFP-containing MVs. Photon flux (photons/s) is plotted over time (days). Error bars represent SEM. ($n = 8$). (*C*) Bioluminescence microscopic images of the recipient HEK293FT cells treated with the Luc–RFP-containing EVs. (Scale bar, 100 μm.) (*D*) The amount of Luc–RFP mRNA in EVs was determined by qRT-PCR. GAPDH was used as an internal control. Error bars represent SD ($n = 3$). (*E*) Analysis of fragmentation of Luc–RFP-encoding mRNAs in EVs by RT-PCR. Four primer sets and their amplified products are indicated below. (*F*) PCR amplification of the entire *Luc* ORF in EVs with and without Luc–RFP-encoding pDNAs. Equal amounts of OD_{260} were PCR amplified. (*G*) Analysis of MV-mediated biomolecule transfer. Recipient cells were treated with actinomycin D (1.0 μg/mL) or cycloheximide (100 μM) to inhibit transcription or translation, respectively. Transfection with purified *Luc* mRNA was used as a control of Act D treatment. Color scale: radiance (x10^5 photons/cm^2/s/sr). (*H*) Analysis of degradation of delivered mRNA in the recipient cells. HEK293FT cells were incubated for 24 h with MVs derived from 4T1 cells stably expressing Luc, and, after removing nonadherent MVs, cultured for another 24 h. GAPDH was amplified as an internal control of recipient cell mRNA.

To initially explain the differential delivery of biomolecules by exosomes and MVs, we determined which nucleic acids encoding reporter genes had been loaded into exosomes and MVs. First, we analyzed Luc–RFP-encoding mRNA in exosomes and MVs derived from HEK293FT cells transiently expressing Luc–RFP. Total RNA was isolated from the exosomes and MVs, and quantitative reverse transcription-PCR (qRT-PCR) was performed for *Luc*. GAPDH mRNA was used to normalize the amount of PCR product. The amount of *Luc–RFP* mRNA in MVs was 3.83 ± 1.28 (average ± SD) times greater than that in exosomes relative to GAPDH (Fig. 3*D*). The lower relative levels of *Luc–RFP* mRNA in exosomes may have been due to preferential mRNA loading, which can be affected by 3′ untranslated regions of the mRNA molecule, and may disfavor reporter mRNA loading; this preferential loading has been previously described (23). The *Luc–RFP* mRNA is derived from a recombinant construct that does not have the 3′ untranslated sequences necessary for efficient loading into the exosome pathway (23). *Luc–RFP* mRNA was detected in exosomes, albeit at levels lower than MVs; nonetheless, there was no detectable induction of reporter protein expression in cells treated with exosomes loaded with *Luc–RFP* mRNA.

Because tumor-derived exosomes contain fragmented ribosomal RNA (24) and genomic DNA (25–27), we anticipated fragmentation of the reporter mRNA in exosomes. We therefore examined the integrity of *Luc–RFP* mRNA in MVs via RT-PCR using four sets of primers along the *Luc* coding region, shown in Fig. 3*E*. All of the four fragments were amplified specifically in both EV types, suggesting that no significant fragmentation of *Luc–RFP* mRNA occurred during EV biogenesis in HEK293FT cells (Fig. 3*E*).

We also examined the loading of Luc–RFP-encoding pDNA into EVs by PCR using the isolated EVs. Interestingly, reporter-encoding pDNA was detected, but only in MVs (Fig. 3*F*). Next, we asked whether the pDNA or mRNA delivered via MVs to reporter cells was the predominant source of *Luc* expression. For this purpose, recipient cells were either treated with actinomycin D (Act D, a transcriptional inhibitor) (28) or cycloheximide (CHX, a translational inhibitor) (29, 30). As a control for pDNA delivery, HEK293FT cells were transfected with *Luc*-encoding pDNA by lipofection (Lipofectamine 2000) and similarly analyzed. As expected, treatment with Act D or CHX completely inhibited expression of the Luc–RFP protein in the cells transfected with pDNA in the cationic lipid formulation (Fig. 3*G*). Both Act D and CHX treatments also completely inhibited expression of Luc–RFP protein in recipient cells treated with MVs derived from HEK293FT cells (Fig. 3*G*; $n = 3$). When we transfected HEK293FT cells with purified *Luc* mRNA by lipofection as a control for mRNA delivery, Act D treatment weakly inhibited expression of Luc–RFP protein by 26.5 ± 3.4% (average ± SD) (Fig. 3*G*). These results suggest that MV-mediated Luc–RFP expression in the recipient cells is mainly induced by delivered pDNA, and not by mRNA.

Next, we investigated the fate of delivered reporter mRNA using murine 4T1 breast cancer cells stably expressing Luc and EGFP as a source of EVs to exclude the effects of pDNA on reporter protein expression. We first confirmed loading of EGFP into EVs by fluorescence microscopy. MVs isolated from the 4T1 cells could be easily visualized in the green fluorescence channel (*SI Appendix*, Fig. S7*B*). In contrast to EVs derived from HEK293FT cells transiently expressing Luc–RFP, EGFP was inefficiently loaded into exosomes isolated from stable 4T1 transfectants (*SI Appendix*, Fig. S7*A*), which is in agreement with differences in EV from different cell types. The loading efficiencies of reporter protein were estimated by assessing luciferase activity showing that MVs contained 4.1 times more Luc protein than exosomes (*SI Appendix*, Fig. S7*C*). To assay for full-length Luc-encoding mRNA, we isolated RNA from EVs derived from the stable transfectants, followed by DNaseI treatment to prevent genomic DNA contamination, and amplified Luc coding region in an RT-PCR using Luc-specific primers. Intact *Luc* mRNA was detected both in exosomes and MVs (*SI Appendix*, Fig. S7*D*).

We next examined whether these EVs could also induce reporter protein expression in recipient cells. Although these

exosomes and MVs contained intact *Luc* mRNA, neither type of EVs induced detectable bioluminescence in recipient HEK293FT cells. We hypothesized that delivered mRNA might be rapidly degraded in the endosome/lysosome compartment without being translated. To test this possibility, recipient HEK293FT cells were treated for 24 h with MVs derived from 4T1 cells stably expressing Luc, and after removing MVs that were not associated with HEK293FT cells, the cultures were incubated for another 24 h. RNA was isolated from the cells at 24 h and 48 h, and RT-PCR was performed for *Luc* mRNA and human *GAPDH* mRNA, an internal control for the recipient HEK293FT transcript. This PCR required high sensitivity and specificity to detect delivered *Luc* mRNA, so we performed two rounds of PCR with a nested set of primers (nested PCR), in which the amplicon from the first PCR was used as a template for the second round of PCR that used a primer set internal to the first set. The amplicon was designed to be the full-length *Luc* mRNA. As expected, *Luc* mRNA was detected in recipient cells only at the 24-h time point, not at 48 h (Fig. 3*H*), indicating that *Luc* mRNA was delivered via MVs to the recipient cells, but likely degraded in intracellular compartments before any significant translation. In this context, internalized exosomes may interact with acidic vesicles such as endosomes/lysosomes (31, 32), in which degradation of the mRNA may occur.

To test this possibility, the localization of the RFP-containing EVs taken up by the recipient cells was studied by confocal fluorescence microscopy. Long-term loading with FITC-dextran specifically labels the endocytic compartments (33, 34). Some of the RFP-containing exosomes and MVs colocalized with the endocytic compartments of the recipient cells (*SI Appendix*, Fig. S8*A*). To further analyze the EV-mediated biomolecular transfer, we applied a lysosome inhibitor, concanamycin A (Con A), which blocks vacuolar acidification through inhibition of V-type ATPases (35). Recipient HEK293FT cells were cultured with Luc–RFP exosomes or MVs in the presence of 50 nM Con A, and the cells containing punctate fluorescent signals, due to the transfer of the reporter protein, were counted (*SI Appendix*, Fig. S8*B*). After 48 h, EV-treated cells cultured in the absence of Con A displayed no detectable signals, whereas in the presence of Con A, over 80% of recipient cells treated with either exosomes or MVs displayed a punctate RFP signal (*SI Appendix*, Fig. S8*C*). This result indicates the degradation of reporter proteins delivered by EVs is dependent on lysosomal acidification.

Because exosomes have been shown to deliver functional small RNAs such as siRNA/shRNA and miRNA to recipient cells (36), we next investigated small RNA delivery via EVs in our system. First we evaluated loading of siRNA into EVs using fluorescently labeled siRNA. HEK293FT cells were transfected with fluorescent siRNAs by lipofection (Lipofectamine 2000), and exosomes and MVs were isolated as described above. siRNA loading was evaluated by fluorescence microscopy. Both exosomes and MVs encapsulated the fluorescent siRNA, although by fluorescence intensity of siRNA loading into exosomes appeared significantly less efficient relative to loading of MVs (*SI Appendix*, Fig. S9*A*). Next, the uptake of siRNA-containing EVs was evaluated by culturing loaded EVs with recipient HEK293FT cells for 24 h. Both types of EVs were taken up by the recipient cells, albeit the fluorescence from exosome-treated cells was far weaker than that of MV-treated cells, likely due to inefficient prior loading of the siRNA into exosomes (*SI Appendix*, Fig. S9*B*).

To evaluate whether the transferred siRNA was functional, siRNA directed against the *Luc* gene (siLuc) was loaded into EVs derived from HEK293FT cells, and delivered to reporter HaCaTs (an immortalized human keratinocyte cell line) stably expressing Luc (37, 38). First, we verified efficient silencing of Luc expression in the reporter HaCaTs by transfecting them with siLuc using Lipofectamine 2000. BLI showed that *Luc* expression in HaCaTs was reduced to 18.0 ± 3.3% (average ± SD) at 48 h after transfection with siLuc, compared with the cells treated likewise with control siRNA (*SI Appendix*, Fig. S9*C*). Next, reporter HaCaTs were treated with siLuc-containing EVs derived from HEK293FT cells and reduction of *Luc* expression was estimated by BLI 48 h later. Neither exosomes nor MVs loaded with targeted siRNA showed significant reduction of Luc expression (*SI Appendix*, Fig. S9*D*). These results demonstrated that loading and delivery of siLuc was more efficient in MVs than exosomes, but that the siRNA delivered by MVs was nonetheless not capable of appreciably reducing Luc expression in the target cells under the conditions tested here.

To investigate a possible correlation between the size of pDNA delivered via MVs and the expression of reporter molecules in recipient cells, we transfected equimolar amounts of pcDNA3.1(+) vector (Invitrogen) encoding either Luc alone or the larger Luc–RFP fusion protein into HEK293FT cells and made the corresponding MVs. We treated recipient HEK293FT cells with these MVs and evaluated the relative efficiency of Luc transfer by BLI (*SI Appendix*, Fig. S10*A*). MVs containing Luc-encoding pDNA alone induced a peak bioluminescence signal in the recipient cells 5.2 times stronger than that induced by MVs containing the larger Luc–RFP-encoding plasmid (*SI Appendix*, Fig. S10*B*). This result suggests that smaller pDNAs can be more efficiently loaded into, and delivered by MVs. Regardless of the use of smaller pDNA, however, exosomes derived from HEK293FT cells transiently transfected to express Luc did not induce detectable bioluminescence in recipient cells (*SI Appendix*, Fig. S10*A*). Lastly, we evaluated exosome-mediated pDNA delivery using the smaller and brighter *Gaussia* luciferase (GLuc) encoded by the same pcDNA3.1(+) vector. GLuc generates over 1,000-fold stronger signal intensity from cells in culture than the more commonly used *Renilla* and firefly luciferases (39). However, exosomes derived from HEK293FT cells transiently transfected with pcDNA3.1(+)-GLuc did not induce bioluminescence in the recipient cells significantly above the background signal (*SI Appendix*, Fig. S10*C*). These results suggested that the size of the delivered pDNA is important for efficient delivery of pDNA via MVs, but that the size of pDNA we used was either too large to be loaded in and delivered by exosomes or that exosomes cannot package pDNA.

One potential caveat is that our MV preparation may have coisolated apoptotic bodies (ABs), which have been shown to package and transfer nucleic acids (40). ABs are 1–5 μm in diameter and secreted through budding from the plasma membrane of apoptotic cells (41). Therefore, to remove potentially copurifying ABs, the supernatant harvested from the cells transiently expressing Luc was centrifuged at 600 × *g*, followed by centrifugation at 2,000 × *g* before isolating MVs as reported (42). This MV preparation led to Luc expression in the recipient cells without significant difference in intensity of bioluminescence, compared with the MVs prepared following our previous protocol (*SI Appendix*, Fig. S11). Therefore, ABs as operationally defined as larger particles removable at 2,000 × *g* were not responsible for the nucleic acid transfer that we are reporting here.

MV-Mediated pDNA Delivery to Visualize Functional Biomolecule Transfer in Vivo via Tumor Cell-Derived MVs to Cells in Organs and Tissues. Tumor cells are thought to release EVs that affect normal cells and tissues, both locally and at a distance, where they may prepare a premetastatic niche (6, 11, 21, 43, 44). MV-mediated pDNA delivery may therefore have utility for the study of the intercellular communication between tumor cells and cells resident in normal tissues, as well as directed molecular therapies. To demonstrate functional biomolecule transfer via tumor cell-derived MVs, we transiently transfected 4T1 murine breast cancer cells with Luc-encoding pDNA and harvested MVs from them. These MVs generated bioluminescence in recipient HEK293 cells that increased over 3 d (*SI Appendix*, Fig. S12 *A* and *B*) similar to previous results, whereas exosomes derived from the same donor

cells induced no detectable Luc signal (*SI Appendix*, Fig. S12*A*). These results demonstrated that the murine breast cancer cells, which form lethal tumors in BALB/c mice, show the same EV-mediated delivery patterns as those from HEK293FT cells.

To reveal long-distance intercellular communication in vivo, we developed a persistent labeling and visualization system for MV-mediated biomolecule transfer by using Cre-lox recombination, which is widely used to carry out DNA excision, inversion, or interchromosomal recombination (45–47). HEK293 cells that have Cre-lox Luc reporter genes integrated in their genome were used as recipient cells to test the reporter system in vitro before animal studies. This construct contains a translational stop signal flanked by *loxP* sites upstream of a *luc* gene; thus, Luc is not expressed until Cre recombinase removes the translational stop signal (48). Cre recombinase-encoding pDNA was delivered via MVs derived from transfected 4T1 cells. These MVs successfully induced site-specific genome recombination, resulting in Luc expression in the recipient reporter HEK293 cells (Fig. 4*A*). Although the reporter cells also showed minimal leaky expression in the absence of MV treatment, the intensity of peak expression of Luc in the recipients on day 3 was 7.7 times stronger than that of the reporter cells without MV treatment (Fig. 4*B*). In contrast, when exosomes were used, the signal was indistinguishable from background (Fig. 4*B*).

We then tested the in vivo transfer of functional biomolecules via tumor cell-derived MVs using Cre-lox Luc reporter mice and

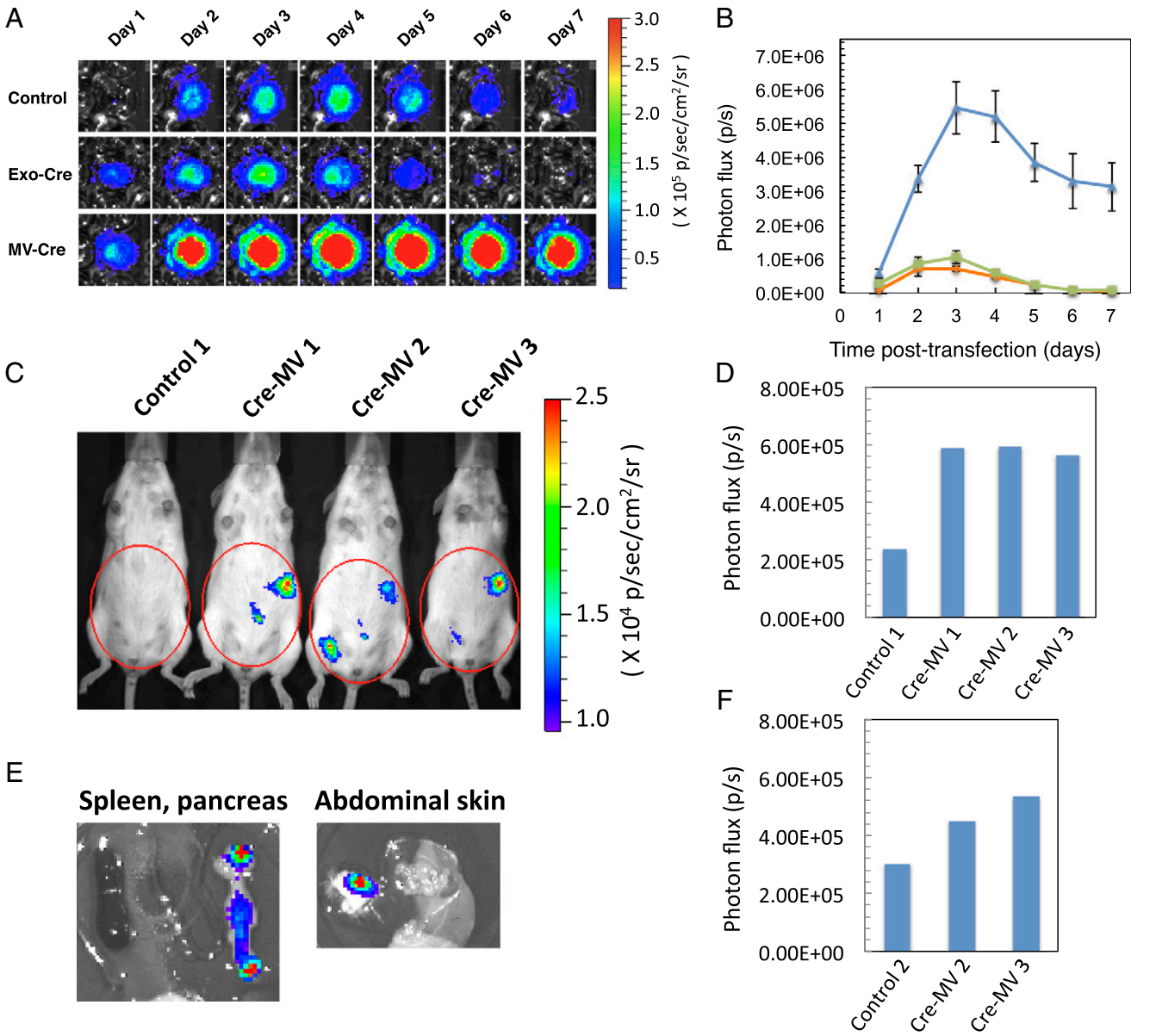

Fig. 4. Imaging of functional biomolecule transfer by tumor cell-derived MVs. (*A*) In vitro activation of Cre-lox reporter cells with MVs from Cre recombinase-expressing cells. Reporter HEK293 cells were treated with 0.5 μg MVs derived from 4T1 cells transiently expressing Cre recombinase. (*B*) Time course of *A*. HEK293 Cre-lox Luc reporter cells were treated with Cre-containing exosomes (green), MVs (blue), or left untreated (orange), and photon emission from individual wells was imaged and quantitated as described above. Error bars represent SEM ($n = 8$). (*C*) Approximately 6 μg Met-1 cell-derived MVs that contain Cre recombinase were injected i.v. into Cre-lox Luc reporter mice. Color scale is radiance (x10^4 photons/cm^2/s/sr). (*D*) Analysis of the bioluminescence from the abdominal regions (red circles indicated in *C*) 48 h after the MV injection. (*E*) Luc expression was measured in excised spleen, pancreas, and abdominal skin. (*F*) Analysis of the bioluminescence from the abdominal regions (red circles indicated in *SI Appendix*, Fig. S13) on day 21.

BLI (48). For this purpose, murine breast cancer cells (strain MET-1), which are syngeneic (MHC H-2k^q) to the reporter mice derived from the friend virus B strain of mice (49), were used as donor cells. MVs that contain Cre-encoding pDNA were prepared from transiently transfected MET-1 cells and injected i.v. into the reporter mice. MVs with Cre-encoding pDNA induced Luc expression at 48 h as assessed by in vivo BLI. A representative example image is shown in Fig. 4*C*. Bioluminescence signals were observed in the abdominal region of all of the reporter mice ($n = 3$), with an average of 2.5 times greater than that of the control (Fig. 4 *C* and *D*). After killing one of the animals at 48 h posttransfer, the excised pancreas and the skin of the abdominal wall had foci of strong Luc expression (Fig. 4*E*). Although it remains to be determined precisely which types of cells expressed Luc in this particular reporter mouse strain, the signal remained for at least 21 d (Fig. 4*F* and *SI Appendix*, Fig. S13), suggesting stable expression. Regardless of the details of this specific system, which may depend on such variables as differential cell surface interactions and promoter activity, this result clearly demonstrates that functional MV-mediated pDNA delivery can be visualized in vivo.

Discussion

Whereas the nature and origins of exosomes and MVs remain to be fully defined, we used standard isolation procedures to generate exosomes and MVs from HEK293FT cells for the purposes of comparing these EVs. The method of differential centrifugation was used and the two populations were thus operationally defined. Nonetheless, the exosomes and MVs were functionally and structurally distinct and had different molecular compositions. There were differences in charge, size, and composition. Importantly, the size distributions of exosomes and MVs overlap significantly, and so size alone cannot always be used to distinguish these EVs from one another. We showed that nucleic acids are differentially loaded into the EVs we defined as exosomes and MVs, and that only MVs can transfer functional pDNA that leads to expression of reporter biomolecules. Reporter-encoding or modulating nucleic acids including pDNA, mRNA, and siRNA are more efficiently loaded into MVs than into exosomes, suggesting that exosomes may restrict encapsulation of nucleic acid cargos to those with unique signatures, as has been recently reported (13, 23). Intact mRNAs were found loaded into both types of EVs, but 24 h after being taken up by recipient cells, transferred mRNAs were degraded in the recipient cells without being effectively translated. In contrast, reporter protein expression could be transferred via MV-mediated delivery of pDNA; however, exosomes failed to package pDNA and could therefore not transfer reporter expression. Regarding the differential delivery of pDNA and mRNA, there is evidence that tumor-derived ABs transfer fragments of functional chromosomal DNAs to nuclei in the surrounding cells (40). This evidence suggests that chromosomal DNAs delivered via ABs can be transported from endosomes to the cell nucleus because ABs are taken up into endosomes by pinocytosis. ABs display negatively charged phospholipid, PS, on the outer membrane leaflet and are macropinocytosed by professional phagocytes and other cell types through this surface-exposed PS (50–52). Similar to the lipid composition of ABs, the MVs in this study also expose PS on their outer membrane leaflet, due to membrane budding that likely occurs during MV biogenesis. Taken together, the similarities between ABs and MVs and our findings suggest that pDNA transferred via MVs could be transported from endosomes to the nucleus of recipient cells and transcribed there into mRNA for protein expression, whereas RNAs in the EVs are likely degraded in the endosome somewhere within this transport pathway. In this context, it would be interesting to determine if genomic DNA fragments could be encapsulated in MVs, transferred to other cells, and expressed in recipient cells as has been described for ABs (40). To date, we have not observed such transfer, despite repeated efforts using consistent model systems and protocols. Perhaps the difference lies in the fact that chromosomal DNA becomes fragmented primarily during apoptosis, and such fragmentation does not occur in our studies. Interestingly, EVs from cancer patients have recently been shown to contain genomic DNA fragments (25–27) that may be derived from the fragmented chromosomes of tumor cells undergoing apoptosis.

Protein expression induced by MV-mediated pDNA delivery is a slower process than after transfection using cationic lipid complexes, which are thought to fuse with the endosomal membrane followed by release of nucleic acid contents into the cytosol (22). This suggests that the MV-mediated DNA transfer we observed is not due to residual lipofection materials; however, because we only used lipofection for pDNA transfer we cannot rule out that the lipofection process leads to pDNA in the MV fraction. Any EV purified from cells that are transiently transfected using lipofection likely contain pDNA in addition to mRNA and protein; therefore, pDNA as a mediator of function needs to be considered for all data reported for macromolecular transfer by EVs. Because MVs functionally deliver DNA but not RNAs, studies of EVs from transiently transfected cells, relative to stably expressing cells, may be confounded by a predominance of pDNA transfer. Further studies of the nature of this transfer will no doubt reveal the specifics of pDNA loading pathways and delivery mechanisms.

Our data support the hypothesis that nucleic acid cargos delivered via MVs stay inside endosomes. Argonaute 2 (Ago2), a component of the RNA-induced silencing complex (RISC), localizes in CD63-containing EVs and binds to miRNA to protect it from degradation by RNase (53–55). This protection mechanism, which is required for functional RNA transfer to recipient cells, does not likely exist for MVs.

Taking advantage of the MV-mediated pDNA delivery, we visualized MV-mediated functional transfer of biomolecules via tumor cell-derived MVs in vivo using BLI as a means of locating where tumor cells communicate with distant cells. Recently, accurate spatiotemporal information regarding the in vivo distribution of exosomes has been obtained by elaborate protein engineering of the exosome surface (56, 57). These studies showed that injected exosomes are trapped in organs such as the liver, spleen, lungs, and kidneys, but it is difficult to directly analyze uptake of the exosomes by cells in these organs. In this regard, MV-mediated pDNA delivery enabled direct in vivo analysis of functional biomolecule transfer via MVs; however, the exosome-mediated functional biomolecule transfer cannot be visualized. In addition, an imaging strategy based on Cre-lox recombination leads to permanent chromosomal rearrangements and stable reporter expression in cells that take up tumor-released MVs in vivo and allows them to be localized and traced over time in a given animal subject. Subsequently, these recipient cells may be identified by analyzing excised bioluminescent tissues. However, due to the differences between specific strains of reporter mice and particulars of expression strategies, the definitive characterization of uptake and expression patterns will require a comprehensive comparison of several models.

A number of studies indicate that EVs may play a role in cancer progression. For example, melanoma or breast tumor-derived exosomes are thought to promote proangiogenic events and modify the extracellular matrix to develop the premetastatic site (11, 21, 43, 44). Conversely, exosomes secreted from surrounding cells may modulate the characteristics of metastatic breast cancer cells (58, 59). Also, tumor-derived EVs may promote immune escape of tumors by inducing the expansion of regulatory T cells, whereas FasL-exposed EVs may induce apoptosis in activated antitumor cytotoxic T and natural killer cells, thereby abrogating this immune checkpoint of tumor growth (60–64). Imaging the functional transfer of biomolecules via tumor-derived MVs will

enable a detailed investigation of how these intercellular communication mechanisms contribute to tumor progression.

In conclusion, previous studies have demonstrated the functional transfer of small RNAs (4, 7–9, 11, 36), mRNA (4, 7, 65, 66), and proteins (5, 6, 10, 21), and a number of other functions of exosomes and MVs (1–3, 60–62) have been reported. However, our results indicate that pDNA transfer, using EVs transiently transfected cells, needs to be considered. A recent report by Chevillet et al. (67) suggests that the unambiguous preparation of EVs, and the mechanisms and consequences of EV-mediated delivery, may be highly dependent on the systems and cell types used, and that these processes are as of yet incompletely understood. Our data are both in agreement with these observations and in addition, demonstrated unique structural and functional attributes of EV populations.

Methods

pDNA, mRNA, and siRNA. For the biomolecule transfer experiments, we used a cDNA encoding a fusion protein of a modified firefly luciferase, Luc 2 (Promega) and tandem Tomato red fluorescent protein (a kind gift from Roger Tsien, University of California, San Diego) cloned into the pcDNA3.1(+) vector under control of the CMV-IE-promoter (Invitrogen/Life Technologies; available from Addgene, plasmid no. 32904) (68). *Luc2*, and humanized *Gaussia Luc* without its signal sequence, were amplified by PCR using (forward) 5′-TGGAATTCTGCAGATGCCGCCACCATGGAAGATGCCAAAAACATTAAGAAGGGCCCA and (reverse) 5′-GCCACTGTGCTGGATTTACACGGCGATCTTGCCGCCCTT, as well as (forward) 5′-TGGAATTCTGCAGATGCCGCCACCATGAAGCCCACCGAGAACAACGAAGACT and (reverse) 5′-GCCACTGTGCTGGATTTAGTCACCACCGGCCCCCTTGATCTT primer sets, respectively. Amplified DNAs were inserted into the EcoRV site of the multiple cloning site of the pcDNA3.1(+)/Neo vector (Invitrogen) by recombination cloning (In-Fusion HD Cloning kit, Clontech). For in vitro *Luc2* mRNA synthesis, *Luc2* cDNA was inserted into pUC19, which contains a T7 polymerase promoter region, and the full sequence was PCR amplified to obtain linearized DNA. The linearized DNA was used as a template for in vitro transcription using the mMessage mMachine kit (Invitrogen) according to the manufacturer's instructions. For the siRNA delivery experiments, the double stranded siRNAs targeting *Luc* mRNA expressed in HaCaTs were (forward) 5′-UAACGAUCCACGACGUAAAUU and (reverse) 5′-UUUACGUCGUGGAUCGUUAUU. Control siRNAs were (forward) 5′-CCCUCAAAAACAAGUUUGCUU and (reverse) 5′-GCAAACUUGUUUUUGAGGGUU (69). Fluorescently labeled siRNA (siGLO cyclophilin B control siRNA) was obtained from Thermo Scientific.

Cells. HEK293FT cells (R700-07, Invitrogen), 4T1 cells, and MET-1 cells were cultured in Dulbecco's modified eagle medium supplemented with GlutaMax (DMEM; Life Technologies), 10% (vol/vol) FBS and 1% penicillin/streptomycin, and incubated at 37 °C in a 5% CO_2 atmosphere.

EV Isolation and Loading Reporter Molecules. EV-depleted medium was prepared by overnight ultracentrifugation of DMEM/10% (vol/vol) FBS at 100,000 × *g*, 4 °C as described (70). Cells were seeded at 1–2 × 10^6 cells per 10-cm dish and cultured for 2 d in 10 mL of EV-free media, and exosomes and MVs were harvested as described with slight modifications (4, 7). Briefly, conditioned medium from a 10-cm cell culture dish was centrifuged at 600 × *g* for 30 min to remove cells and debris. The supernatant was ultracentrifuged at 20,000 × *g* for 30 min to pellet MVs. Supernatants thereof were filtered through 0.2-μm membrane filters (Thermo Scientific) with pressure to remove vesicles larger than 200 nm in diameter. Finally, exosomes were collected by ultracentrifugation at 100,000 × *g* for 90 min using Optima XL-90 Ultracentrifuge and a 90Ti rotor (Beckman Coulter). Isolated EVs were quantified by measuring their protein concentration (DC Protein Assay, Bio Rad) and stored at −80 °C until needed.

Transfections. For efficient loading of pDNA/mRNA or siRNA into EVs, cells were transfected with pDNA encoding reporter molecules or siRNA using lipofection (Lipofectamine 2000, Invitrogen/Life Technologies), with a modified transfection protocol to obtain higher expression levels of the reporter molecules. Briefly, donor cells were incubated with lipofectamine/pDNA or siRNA complexes in DMEM without FBS and penicillin/streptomycin for 8–12 h, after which the transfection medium was replaced with 10 mL EV-depleted media, followed by culturing the cells for 2 d and EV isolation as described below.

Polyethylene Glycol Precipitation of EVs. Isolated EVs were precipitated with polyethylene glycol (PEG buffer) as reported with slight modifications (71). The isolated exosomes and MVs were resuspended in 10% (wt/vol) PEG 8000/PBS and incubated overnight at 4 °C. EVs were precipitated by centrifugation at 1,500 × *g* for 30 min. After removing supernatant, residual supernatant was eliminated by centrifugation at 1,500 × *g* for 5 min. The resulting EV pellet was resuspended in PBS. This is similar to commercially available EV isolation kits.

DLS Measurement. EVs derived from HEK293FT cells were sized using the Zetasizer Nano ZS90 (Malvern Instruments).

NTA Measurement. NTA was carried out using the ZetaView Multiple Parameter Particle Tracking Analyzer (Particle Metrix). EVs resuspended in PBS were further diluted 100- to 500-fold for measurement. The diffusion constant was calculated from the direct observation of Brownian motion and transferred into a size histogram via the Einstein–Stokes relation between diffusion constant and particle size.

AFM. EVs were incubated on freshly cleaved mica surfaces with or without 10 mM $MgCl_2$ for 30 min and diluted 20-fold with PBS. An AFM system (NX10, Park System) equipped with an in-fluid probe holder was used to image the EVs in PBS buffer by tapping mode AFM. Soft AFM cantilevers with spring constants of ∼0.1 N/m (SHOCONG, AppNano) were driven at ∼6 kHz during tapping mode scans. All images were acquired at room temperature with 5-μm scan width, 1-Hz scan rate, and set point = 70–80% of the free amplitude. Volumes of EVs were quantified using ImageJ software (Research Services Branch, National Institute of Mental Health; imagej.nih.gov/).

Western Blotting. EVs derived from HEK293FT cells were mixed with 2× sample buffer [125 mM Tris·HCl pH 6.8, 4% (wt/vol) SDS, 20% (vol/vol) glycerol, 100 mM DTT, 0.01% bromophenol blue], and heated at 90 °C for 10 min. Proteins were separated on a 10% Mini-PROTEAN TGX gel (Bio-Rad) and transferred to a nitrocellulose membrane (Bio-Rad). CD63 was detected with the CD63 ExoAB Antibody kit (EXOAB-CD63A-1, System Biosciences). Human GAPDH was detected with anti-GAPDH antibody (G9545, Sigma).

Total RNA Isolation, Reverse Transcription, and qRT-PCR. Total RNA was extracted from EVs with an RNeasy mini kit (Qiagen), and purity and concentration of the isolated RNA were measured using a Nanodrop-1000 Spectrophotometer (Thermo Scientific). cDNA was synthesized with SuperScript III Reverse Transcriptase (Invitrogen/Life Technologies) using oligo(dT) primers, and real-time PCR was performed on 7500 Fast Real-Time PCR system (Life Technologies) using SYBR Green PCR Master Mix (Life Technologies) with primers specific for Luc2 and GAPDH. *Luc2* was amplified using primers (forward) 5′-CTACTTGATCTGCGGCTTTCG and (reverse) 5′-AGCAGGGCAGATTGAATCTTATAGTCT, and *GAPDH* was amplified using (forward) 5′-GGGTGTGAACCATGAGAAGT and (reverse) 5′-GGCATGGACTGTGGTCATGA primers. Transcript levels were normalized to the level of GAPDH mRNA. The comparative quantitation method (ΔΔCt) was used to compare the different samples and transform them to absolute values with $2^{-\Delta\Delta Ct}$ for obtaining relative fold changes.

Analysis of mRNA Fragmentation/Degradation. Four primer sets were used to analyze fragmentation of Luc2-encoding mRNA transiently expressed in HEK293FT cells (shown in Fig. 3*E*): (forward) 1 and 2, 5′-TGGAATTCTGCAGATGCCGCCACCATGGAAGATGCCAAAAACATTAAGAAGGGCCCA and (reverse) 1, 5′-GCCACTGTGCTGGATTTACACGGCGATCTTGCCGCCCTT and (reverse) 2, 5′-AGCAGGGCAGATTGAATCTTATAGTCT; (forward) 3, 5′-CTACTTGATCTGCGGCTTTCG and (reverse) 3, 5′-GTCGAAGATGTTGGGGTGTT; and (forward) 4, 5′-GGACTTGGACACCGGTAAGA and (reverse) 4, 5′-GCCACTGTGCTGGATTTACACGGCGATCTTGCCGCCCTT. PCR was performed using Platinum Taq DNA Polymerase (Invitrogen) or CloneAmp HiFi PCR Premix (Clontech). Full-length Luc stably expressed in 4T1 cells (72) was amplified using (forward) 5′-ATGGAGGATGCCAAGAATATTAAGA and (reverse) 5′-TTACACAGCAATTTTGCCACCCTTC primers. To analyze mRNA degradation, nested PCR was performed using (forward) 5′-GCTGTGGCAAAGAGGTTCCATC and (reverse) 5′-GTCTTTCCATGCTCCAGAACCAC primers. GAPDH was amplified using (forward) 5′-GGGTGTGAACCATGAGAAGT and (reverse) 5′-GGCATGGACTGTGGTCATGA primers (Fig. 3*H*). To avoid contamination of Luc-encoding DNA integrated in the genomic DNA, isolated total RNA was treated with DNaseI (Invitrogen) before reverse transcription.

Analysis of pDNA Loaded in EVs. After isolating EVs, the amount of nucleic acid contained was estimated by measuring the absorbance at 260 nm, using a Nanodrop-1000 Spectrophotometer (Thermo Scientific). Equal amounts of OD_{260} were used for each PCR.

EV Bead Coupling and Flow Cytometry. Antibody-coated beads were prepared as previously described (73). A total of 4 μm aldehyde/sulfate latex beads (A37304, Life Technologies) was incubated with anti-CD63 antibody (556019, BD Pharmingen) overnight at room temperature in MES buffer (2.5 mM, pH 6). RFP-containing EVs were washed using PEG precipitation. A total of 0.13 μg exosomes or MVs were incubated with anti-CD63 beads for 15 min at room temperature with shaking; after the volume was filled up to 400 μL, the EV-bead mixture was incubated for 3.5 h at room temperature. A total of 400 μL of 100 mM glycine was added and incubated at room temperature for 35 min to block remaining binding sites. After washing the EV-coated beads twice with PBS/5% (wt/vol) BSA, EV-coated beads were resuspended in PBS. Flow cytometry data were collected on a Facscan (excitation 561 nm, emission 615/25 nm) and analyzed with FlowJo software (Tree Star).

Analysis of Reporter Protein Loading into EVs and Protein Transfer to Recipient Cells. Isolated EVs or cells treated with EVs were lysed by adding 0.2% Triton X-100 (T-8787, Sigma-Aldrich) in PBS. The amount of Luc proteins was estimated using the Luciferase Assay System (E1501, Promega).

Fluorescence Microscopy. Phase contrast and fluorescence images were taken using an EVOS FL Cell Imaging System (Life Technologies). Cells or EVs were observed using the Nunc Lab-Tek Chamber Slide System (Thermo Scientific). Isolated EVs were labeled with the lipophilic fluorescent dye PKH26 (Sigma-Aldrich), washed with 10 mL PBS, collected by ultracentrifugation as described above, and resuspended in PBS. For the inhibition of lysosomal acidification, concanamycin A (sc-202111, Santa Cruz Biotechnology) was dissolved in DMSO and used at a final concentration of 50 nM for 16 h.

For detection of surface phosphatidylserine, EVs were resuspended in annexin V binding buffer (sc-291903, Santa Cruz Biotechnology) and incubated with 5 μg/mL annexin V-FITC (74) for 12 h until enough numbers of EVs were adsorbed onto the glass surface for fluorescence microscopic analysis. For evaluation of nonspecific binding of FITC with MVs, 100 μM FITC-dextran (FD250S, Sigma-Aldrich) dissolved in PBS was incubated with MVs.

Laser scanning confocal microscopy was carried out using a Leica TCS SP8 confocal microscope (Leica Microsystems) with an objective lens (HC PL APO 40 NA 1.30 oil), which is located in the Cell Sciences Imaging Facility (Stanford University, Stanford, CA). For evaluation of colocalization of EVs and endocytic compartments, HEK293FT cells were cultured with RFP-containing EVs for 18 h, followed by culturing with 5 mg/mL FITC-dextran (FD150S, Sigma-Aldrich) for 2 h. These cells were then washed with PBS three times and incubated for 1 h with culture medium that contains 10 μg/mL Hoechst 33342 (H3570, Life Technologies) before microscopy was performed.

BLI. In vitro or in vivo assays for luciferase expression were performed with IVIS 50 or IVIS 200 systems (Xenogen Product line of Perkin-Elmer), which is located in the Stanford Center for Innovation in In-Vivo Imaging. Microscopic bioluminescence imaging was performed with a LV200 microscope (Olympus). For in vitro assays, D-luciferin (300 μg/mL) or coelenterazine native (20 μM) (303, NanoLight Technology) was added before bioluminescence imaging and emitted light was captured by an IVIS-50 (Perkin-Elmer). For in vivo imaging, animals were anesthetized with isoflurane using an SAS3 anesthesia system (Summit Anesthesia Support) and an EVAC 4 waste gas evacuation system (Universal Vaporizer Support), placed into the light-tight chamber of the CCD camera system (IVIS-200, Perkin-Elmer), and a grayscale body surface reference image (digital photograph) was taken under weak illumination. After switching off the light source, photons emitted from luciferase-expressing cells within the animal body and transmitted through the tissue were quantified over a defined period ranging up to 5 min using the software program Living Image (Perkin-Elmer). For anatomical localization, a pseudocolor image representing light intensity (blue, least intense; red, most intense) was generated in Living Image and superimposed onto the grayscale reference image.

Cre-Lox Reporter Mice. For visualization of EV-mediated reporter delivery, we used a silenced, conditionally activated dual-reporter transgenic mouse previously created to monitor conditional reporter gene activation by in vivo BLI and fluorescence imaging after cross-breeding with Cre-expressing transgenic mice (48). The transgene contains the CAG promoter (75), the coding sequence of *Renilla* luc, and a stop signal sequence (both flanked by loxP sites), followed by the coding sequence of click beetle luciferase fused to humanized Monster GFP (hMGFP). Approximately 6 μg of MVs containing Cre recombinase-encoding pDNA were i.v. injected into the reporter mice. Expression of Luc was analyzed by BLI after intraperitoneally injecting D-luciferin at 150 mg/kg. Experimental protocols were approved by the Stanford Administrative Panel on Laboratory Animal Care.

ACKNOWLEDGMENTS. We thank Dr. R. P. Hickerson, Dr. J. A. Prescher, Dr. Q. Wang, and Dr. J. F. Tait for providing Cre recombinase expression pDNA, Cre-lox reporter cells, and Annexin V-FITC, respectively; Dr. A. Delcayre and Dr. Y. Kato for giving useful suggestions on exosome and microvesicle biology; Dr. R. Zare for generously letting us use the Zetasizer Nano ZS90; and Dr. E. Geihe and Ms. M. Russo for supporting our DLS measurements. This work was supported, in part, by the Japan Society for the Promotion of Science fellowship (to M.K.), the Uehara Memorial Foundation fellowship (to M.K.), an unrestricted gift from the Chambers Family Foundation (to C.H.C.), and by Grant 1UH2TR000902-01 from the National Institutes of Health (to A.C.M. and C.H.C.). We also thank the Olympus Corporation for generously letting us use the LV200 bioluminescence imaging microscope.

1. Raposo G, Stoorvogel W (2013) Extracellular vesicles: Exosomes, microvesicles, and friends. *J Cell Biol* 200(4):373–383.
2. EL Andaloussi S, Mäger I, Breakefield XO, Wood MJ (2013) Extracellular vesicles: Biology and emerging therapeutic opportunities. *Nat Rev Drug Discov* 12(5):347–357.
3. Lee Y, El Andaloussi S, Wood MJA (2012) Exosomes and microvesicles: Extracellular vesicles for genetic information transfer and gene therapy. *Hum Mol Genet* 21(R1): R125–R134.
4. Valadi H, et al. (2007) Exosome-mediated transfer of mRNAs and microRNAs is a novel mechanism of genetic exchange between cells. *Nat Cell Biol* 9(6):654–659.
5. Al-Nedawi K, et al. (2008) Intercellular transfer of the oncogenic receptor EGFRvIII by microvesicles derived from tumour cells. *Nat Cell Biol* 10(5):619–624.
6. Al-Nedawi K, Meehan B, Kerbel RS, Allison AC, Rak J (2009) Endothelial expression of autocrine VEGF upon the uptake of tumor-derived microvesicles containing oncogenic EGFR. *Proc Natl Acad Sci USA* 106(10):3794–3799.
7. Skog J, et al. (2008) Glioblastoma microvesicles transport RNA and proteins that promote tumour growth and provide diagnostic biomarkers. *Nat Cell Biol* 10(12): 1470–1476.
8. Pegtel DM, et al. (2010) Functional delivery of viral miRNAs via exosomes. *Proc Natl Acad Sci USA* 107(14):6328–6333.
9. Mittelbrunn M, et al. (2011) Unidirectional transfer of microRNA-loaded exosomes from T cells to antigen-presenting cells. *Nat Commun* 2:282.
10. Choudhuri K, et al. (2014) Polarized release of T-cell-receptor-enriched microvesicles at the immunological synapse. *Nature* 507(7490):118–123.
11. Zhou W, et al. (2014) Cancer-secreted miR-105 destroys vascular endothelial barriers to promote metastasis. *Cancer Cell* 25(4):501–515.
12. Piccin A, Murphy WG, Smith OP (2007) Circulating microparticles: Pathophysiology and clinical implications. *Blood Rev* 21(3):157–171.
13. Villarroya-Beltri C, et al. (2013) Sumoylated hnRNPA2B1 controls the sorting of miRNAs into exosomes through binding to specific motifs. *Nat Commun* 4:2980.
14. Ghossoub R, et al. (2014) Syntenin-ALIX exosome biogenesis and budding into multivesicular bodies are controlled by ARF6 and PLD2. *Nat Commun* 5:3477.
15. Ostrowski M, et al. (2010) Rab27a and Rab27b control different steps of the exosome secretion pathway. *Nat Cell Biol* 12(1):19–30, 1–13.
16. Gould SJ, Raposo G (2013) As we wait: Coping with an imperfect nomenclature for extracellular vesicles. *J Extracell Vesicles* 2:20389.
17. Heijnen HF, Schiel AE, Fijnheer R, Geuze HJ, Sixma JJ (1999) Activated platelets release two types of membrane vesicles: Microvesicles by surface shedding and exosomes derived from exocytosis of multivesicular bodies and alpha-granules. *Blood* 94(11):3791–3799.
18. Egawa H, Furusawa K (1999) Liposome adhesion on mica surface studied by atomic force microscopy. *Langmuir* 15:1660–1666.
19. Shaner NC, Steinbach PA, Tsien RY (2005) A guide to choosing fluorescent proteins. *Nat Methods* 2(12):905–909.
20. El-Andaloussi S, et al. (2012) Exosome-mediated delivery of siRNA in vitro and in vivo. *Nat Protoc* 7(12):2112–2126.
21. Peinado H, et al. (2012) Melanoma exosomes educate bone marrow progenitor cells toward a pro-metastatic phenotype through MET. *Nat Med* 18(6):883–891.
22. Stegmann T, Legendre JY (1997) Gene transfer mediated by cationic lipids: Lack of a correlation between lipid mixing and transfection. *Biochim Biophys Acta* 1325(1): 71–79.
23. Bolukbasi MF, et al. (2012) miR-1289 and "Zipcode"-like sequence enrich mRNAs in microvesicles. *Mol Ther Nucleic Acids* 1:e10.
24. Jenjaroenpun P, et al. (2013) Characterization of RNA in exosomes secreted by human breast cancer cell lines using next-generation sequencing. *PeerJ* 1:e201.
25. Kahlert C, et al. (2014) Identification of double-stranded genomic DNA spanning all chromosomes with mutated KRAS and p53 DNA in the serum exosomes of patients with pancreatic cancer. *J Biol Chem* 289(7):3869–3875.
26. Lázaro-Ibáñez E, et al. (2014) Different gDNA content in the subpopulations of prostate cancer extracellular vesicles: Apoptotic bodies, microvesicles, and exosomes. *Prostate* 74(14):1379–1390.

27. Thakur BK, et al. (2014) Double-stranded DNA in exosomes: A novel biomarker in cancer detection. *Cell Res* 24(6):766–769.
28. Yung BY, Bor AM, Chan PK (1990) Short exposure to actinomycin D induces "reversible" translocation of protein B23 as well as "reversible" inhibition of cell growth and RNA synthesis in HeLa cells. *Cancer Res* 50(18):5987–5991.
29. Baliga BS, Pronczuk AW, Munro HN (1969) Mechanism of cycloheximide inhibition of protein synthesis in a cell-free system prepared from rat liver. *J Biol Chem* 244(16): 4480–4489.
30. Dai C-L, et al. (2013) Inhibition of protein synthesis alters protein degradation through activation of protein kinase B (AKT). *J Biol Chem* 288(33):23875–23883.
31. Parolini I, et al. (2009) Microenvironmental pH is a key factor for exosome traffic in tumor cells. *J Biol Chem* 284(49):34211–34222.
32. Tian T, Wang Y, Wang H, Zhu Z, Xiao Z (2010) Visualizing of the cellular uptake and intracellular trafficking of exosomes by live-cell microscopy. *J Cell Biochem* 111(2): 488–496.
33. Martinez I, et al. (2000) Synaptotagmin VII regulates Ca(2+)-dependent exocytosis of lysosomes in fibroblasts. *J Cell Biol* 148(6):1141–1149.
34. Jaiswal JK, Andrews NW, Simon SM (2002) Membrane proximal lysosomes are the major vesicles responsible for calcium-dependent exocytosis in nonsecretory cells. *J Cell Biol* 159(4):625–635.
35. Dröse S, Altendorf K (1997) Bafilomycins and concanamycins as inhibitors of V-ATPases and P-ATPases. *J Exp Biol* 200(Pt 1):1–8.
36. Hagiwara K, Ochiya T, Kosaka N (2014) A paradigm shift for extracellular vesicles as small RNA carriers: From cellular waste elimination to therapeutic applications. *Drug Deliv Transl Res* 4(1):31–37.
37. Hickerson RP, et al. (2011) Use of self-delivery siRNAs to inhibit gene expression in an organotypic pachyonychia congenita model. *J Invest Dermatol* 131(5):1037–1044.
38. Geihe EI, et al. (2012) Designed guanidinium-rich amphipathic oligocarbonate molecular transporters complex, deliver and release siRNA in cells. *Proc Natl Acad Sci USA* 109(33):13171–13176.
39. Tannous BA, Kim D-E, Fernandez JL, Weissleder R, Breakefield XO (2005) Codon-optimized Gaussia luciferase cDNA for mammalian gene expression in culture and in vivo. *Mol Ther* 11(3):435–443.
40. Bergsmedh A, et al. (2001) Horizontal transfer of oncogenes by uptake of apoptotic bodies. *Proc Natl Acad Sci USA* 98(11):6407–6411.
41. György B, et al. (2011) Membrane vesicles, current state-of-the-art: Emerging role of extracellular vesicles. *Cell Mol Life Sci* 68(16):2667–2688.
42. Crescitelli R, et al. (2013) Distinct RNA profiles in subpopulations of extracellular vesicles: Apoptotic bodies, microvesicles and exosomes. *J Extracell Vesicles* 2:1–10.
43. Hood JL, San RS, Wickline SA (2011) Exosomes released by melanoma cells prepare sentinel lymph nodes for tumor metastasis. *Cancer Res* 71(11):3792–3801.
44. Kosaka N, et al. (2013) Neutral sphingomyelinase 2 (nSMase2)-dependent exosomal transfer of angiogenic microRNAs regulate cancer cell metastasis. *J Biol Chem* 288(15): 10849–10859.
45. Branda CS, Dymecki SM (2004) Talking about a revolution: The impact of site-specific recombinases on genetic analyses in mice. *Dev Cell* 6(1):7–28.
46. Zong H, Espinosa JS, Su HH, Muzumdar MD, Luo L (2005) Mosaic analysis with double markers in mice. *Cell* 121(3):479–492.
47. Livet J, et al. (2007) Transgenic strategies for combinatorial expression of fluorescent proteins in the nervous system. *Nature* 450(7166):56–62.
48. Gonzalez-Gonzalez E, et al. (2009) siRNA silencing of keratinocyte-specific GFP expression in a transgenic mouse skin model. *Gene Ther* 16(8):963–972.
49. Borowsky AD, et al. (2005) Syngeneic mouse mammary carcinoma cell lines: Two closely related cell lines with divergent metastatic behavior. *Clin Exp Metastasis* 22(1): 47–59.
50. Platt N, da Silva RP, Gordon S (1998) Recognizing death: The phagocytosis of apoptotic cells. *Trends Cell Biol* 8(9):365–372.
51. Henson PM, Bratton DL, Fadok VA (2001) Apoptotic cell removal. *Curr Biol* 11(19): R795–R805.
52. Mercer J, Helenius A (2008) Vaccinia virus uses macropinocytosis and apoptotic mimicry to enter host cells. *Science* 320(5875):531–535.
53. Gibbings DJ, Ciaudo C, Erhardt M, Voinnet O (2009) Multivesicular bodies associate with components of miRNA effector complexes and modulate miRNA activity. *Nat Cell Biol* 11(9):1143–1149.
54. Zhang Y, et al. (2010) Secreted monocytic miR-150 enhances targeted endothelial cell migration. *Mol Cell* 39(1):133–144.
55. Li L, et al. (2012) Argonaute 2 complexes selectively protect the circulating microRNAs in cell-secreted microvesicles. *PLoS ONE* 7(10):e46957.
56. Lai CP, et al. (2014) Dynamic biodistribution of extracellular vesicles in vivo using a multimodal imaging reporter. *ACS Nano* 8(1):483–494.
57. Takahashi Y, et al. (2013) Visualization and in vivo tracking of the exosomes of murine melanoma B16-BL6 cells in mice after intravenous injection. *J Biotechnol* 165(2):77–84.
58. Ono M, et al. (2014) Exosomes from bone marrow mesenchymal stem cells contain a microRNA that promotes dormancy in metastatic breast cancer cells. *Sci Signal* 7(332):ra63.
59. Luga V, et al. (2012) Exosomes mediate stromal mobilization of autocrine Wnt-PCP signaling in breast cancer cell migration. *Cell* 151(7):1542–1556.
60. Wieckowski EU, et al. (2009) Tumor-derived microvesicles promote regulatory T cell expansion and induce apoptosis in tumor-reactive activated CD8+ T lymphocytes. *J Immunol* 183(6):3720–3730.
61. Muralidharan-Chari V, Clancy JW, Sedgwick A, D'Souza-Schorey C (2010) Microvesicles: Mediators of extracellular communication during cancer progression. *J Cell Sci* 123(Pt 10):1603–1611.
62. Zhang H-G, Grizzle WE (2011) Exosomes and cancer: A newly described pathway of immune suppression. *Clin Cancer Res* 17(5):959–964.
63. Valenti R, et al. (2007) Tumor-released microvesicles as vehicles of immunosuppression. *Cancer Res* 67(7):2912–2915.
64. Pardoll DM (2012) The blockade of immune checkpoints in cancer immunotherapy. *Nat Rev Cancer* 12(4):252–264.
65. Mizrak A, et al. (2013) Genetically engineered microvesicles carrying suicide mRNA/protein inhibit schwannoma tumor growth. *Mol Ther* 21(1):101–108.
66. Deregibus MC, et al. (2007) Endothelial progenitor cell derived microvesicles activate an angiogenic program in endothelial cells by a horizontal transfer of mRNA. *Blood* 110(7):2440–2448.
67. Chevillet JR, et al. (2014) Quantitative and stoichiometric analysis of the microRNA content of exosomes. *Proc Natl Acad Sci USA* 111(41):14888–14893.
68. Patel MR, et al. (2010) Longitudinal, noninvasive imaging of T-cell effector function and proliferation in living subjects. *Cancer Res* 70(24):10141–10149.
69. Hickerson RP, et al. (2008) Stability study of unmodified siRNA and relevance to clinical use. *Oligonucleotides* 18(4):345–354.
70. Théry C, Amigorena S, Raposo G, Clayton A (2006) Isolation and characterization of exosomes from cell culture supernatants and biological fluids. *Curr Protoc Cell Biol* Chapter 3:22.
71. Chen L, et al. (2013) Cardiac progenitor-derived exosomes protect ischemic myocardium from acute ischemia/reperfusion injury. *Biochem Biophys Res Commun* 431(3): 566–571.
72. Thorne SH, et al. (2009) CNOB/ChrR6, a new prodrug enzyme cancer chemotherapy. *Mol Cancer Ther* 8(2):333–341.
73. Wahlgren J, et al. (2012) Plasma exosomes can deliver exogenous short interfering RNA to monocytes and lymphocytes. *Nucleic Acids Res* 40(17):e130.
74. Tait JF, et al. (2006) Improved detection of cell death in vivo with annexin V radiolabeled by site-specific methods. *J Nucl Med* 47(9):1546–1553.
75. Sawicki JA, Morris RJ, Monks B, Sakai K, Miyazaki J (1998) A composite CMV-IE enhancer/β-actin promoter is ubiquitously expressed in mouse cutaneous epithelium. *Exp Cell Res* 244(1):367–369.